Proc. 3rd Int. Conf. Physics of Solid State Ionics (ICPSSI-3)
J. Phys. Soc. Jpn. **79** (2010) Suppl. A, pp. 59-64

Atomic Level Investigations of Lithium Ion Battery Cathode Materials

Craig A. J. FISHER*, M. Saiful ISLAM[1] and Hiroki MORIWAKE

Nanostructures Research Laboratory, Japan Fine Ceramics Center, 2-4-1 Mutsuno, Atsuta-ku, Nagoya 456-8587, Japan

[1]*Department of Chemistry, University of Bath, Bath BA2 7AY, U.K.*

(Received November 20, 2009; accepted November 29, 2009)

The defect energetics, ion migration processes and surface structures of lithium ion battery cathode materials $LiCoO_2$ and $LiMPO_4$ (M = Mn, Fe, Co or Ni), probed using a Born model description of atomic interactions, are reported. The lowest energy intrinsic disorder types comprise lithium deficiency in the case of $LiCoO_2$ and cation antisite defects in the case of the orthophosphates. Lithium diffusion in $LiCoO_2$ is confirmed to be two dimensional, with a calculated activation barrier of 0.45 eV, whereas in $LiMPO_4$ compounds diffusion is one dimensional only, with a barrier decreasing from 0.62 to 0.44 eV across the transition metal series. Unlike the linear path calculated for $LiCoO_2$, in orthophosphates the Li ion follows a curved path between vacancies. Examination of low index surfaces in $LiCoO_2$ and $LiFePO_4$ further illustrates the utility of these methods for probing materials systems on the atomic level.

KEYWORDS: Li-ion battery, defect energetics, ion diffusion, surface, crystal morphology

1. Introduction

Materials used in the cathodes of rechargeable lithium ion batteries are of immense interest given their importance in determining the properties of these efficient energy storage devices.[1)] First proposed by Goodenough and coworkers over two decades ago,[2)] $LiCoO_2$ is the most widely used cathode material. However, there remains much that is not understood about its properties, particularly on the atomic level.

Over the last couple of decades, a number of alternative cathode materials have been proposed in an attempt to overcome concerns associated with $LiCoO_2$, such as cost and safety.[1,3)] One such class of materials is the orthophosphate group $LiMPO_4$ (M = Mn, Fe, Co or Ni), the most widely studied of which is $LiFePO_4$.[4,5)] The greater stability of $LiFePO_4$ vis-a-vis $LiCoO_2$ means it can safely be used in large-scale batteries, e.g., in electric vehicles.

Computer simulation techniques offer a powerful means of probing the structure-property relationships in materials at the atomic level, aiding in the interpretation of experimental results and revealing trends to guide materials design strategies. Simulation techniques can provide detailed information, for example, about intrinsic point defect types, relative redox stabilities, propensities for solid-state solution formation, defect clustering, and ion migration mechanisms. Such techniques have been used successfully on a wide-range of inorganic solids, including other lithium battery materials such as spinel-structured $LiMn_2O_4$[6)] and orthosilicate Li_2MnSiO_4.[7)] A number of *ab initio* simulations of both systems have also been reported in the literature, providing details of electronic structure and related properties.[8-14)] In this paper we compare and contrast defect formation, ion migration mechanisms and surfaces in the layered oxide $LiCoO_2$ and orthophosphates $LiMPO_4$, where M = Mn, Fe, Co or Ni, using a classical potential model. The advantage of this model is that it enables the treatment of a much larger number of ions in any given simulation, an important aspect in handling the long-scale perturbations that arise from lattice point defects and surfaces.

2. Methods

2.1 Potential models

The potential energy between pairs of ions in each crystalline solid was calculated by combining the long-range Coulombic component with an analytical function representing short-range repulsive and van der Waals interactions as per the Born-Mayer-Huggins (BMH) potential. The short-range interactions, Φ_{ij}, were modeled using the Buckingham potential:

$$\Phi_{ij}\left(r_{ij}\right) = A_{ij}\exp\left(-r_{ij}/\rho_{ij}\right) - C_{ij}/r_{ij}^{6}, \qquad (1)$$

where r is the distance between ions i and j, and A, ρ and C are potential parameters fitted to reproduce the experimental lattice parameters and ion positions within the unit cell.

In the case of the orthophosphates, an additional 3-body term, $\Phi_{ijk,}$ was used to describe the directional bonding in PO_4 tetrahedra:

$$\Phi_{ijk} = \tfrac{1}{2} K_{ijk}\left(\theta - \theta_0\right)^2. \qquad (2)$$

Here K is the force constant and the angle θ_0 is the equilibrium bond angle for i-j-k triplets centered on ion i.

The effects of electronic polarization of transition metal and oxide ions were approximated using the shell model.[15)] In this model, the ion is divided into a core and shell of different charges connected by a harmonic spring. The polarizability, α, is given by Y^2/k, where Y is the charge on the shell and k is the spring constant. This method has proven effective in simulating dielectric properties of a wide range of ceramic oxides.

Ions were assigned their formal charges in all cases. Employing a formal charge model does not necessarily mean that the electron distribution corresponds to a fully ionic system; the validity of the model is assessed primarily by its ability to reproduce observed crystal properties. The chief advantage of the formal charge model is that there is no

ambiguity about the charge state when considering defects and their associated charge compensation mechanisms.

The potential model used for $LiCoO_2$ is summarized in Table I. The potential parameters for LiMPO$_4$ (M = Mn, Fe, Co or Ni) were identical to those in ref. 16. Phonon calculations using these parameter sets confirmed that the experimental structures corresponded to the room temperature stable phases.

2.2 Defect calculations

Static lattice calculations were performed using the Mott-Littleton method to determine lattice relaxation about point defects and the resultant energy changes. Thermal vibrations were ignored so that the minimum energy, stable states of the different structures could be compared.

The Mott-Littleton method partitions the crystal lattice around the defect center into two regions, with the inner sphere labeled region 1 and the outer sphere labeled region 2a. Atoms outside of these spheres lie in region 2b, which extends to infinity. A radius of 12 Å was used for region 1, corresponding to a sphere of several hundred ions. The forces on ions in this region were calculated explicitly using the BMH potential. In region 2a, the forces were assumed to result from the defect alone. In region 2b the only force acting on the ions was assumed to be Coulombic, so the energy of the region was taken as the induced relaxation energy due to the net charge of the defect center.

2.3 Ion migration

Lithium ion migration energies and pathways were calculated in a similar way to point defects by considering a lithium ion in a series of interstitial positions between two adjacent Li vacancies. The Li ion in each instance was fixed along one coordinate and allowed to relax in the other two directions. In this way any deviation of the minimum energy pathway from a direct linear route could be determined. The local maximum energy along this migration path represents the migration enthalpy.

2.4 Surface simulations

Surfaces of $LiCoO_2$ and $LiFePO_4$ were simulated using a two-region approach for a number of low index planes with the same potential models as for the bulk crystal. In cases where the as-cut crystal had a non-zero dipole moment normal to the surface plane, the surface was modified by moving half the outermost ions to the opposite side of the crystal. Canceling the dipole moment in this way allowed converged surface energies to be obtained upon relaxation. Further details of the method can be found in ref. 17.

Surface energies, $E_{surface}$, were calculated according to

$$E_{surface} = \frac{E_s - E_b}{A} \tag{3}$$

where E_s is the energy of the surface containing region, E_b is the energy of bulk crystal containing the same number of atoms, and A is the surface cross-sectional area. Plotting the surface energies on a Wulff net allows the equilibrium morphology of a crystalline particle to be estimated.

All calculations were performed with the GULP code.[18)]

3. Results and discussion

3.1 Crystal structures

The BMH parameters listed in Table I were fitted to reproduce the structural features of hexagonal $LiCoO_2$ (Fig. 1) using efficient Newton-Raphson minimization techniques. Cation-cation interactions were assumed to be purely Coulombic. The structural parameters of $LiCoO_2$ calculated using these potentials are compared with experiment in Table II.

Table I. BMH parameters used in simulations of $LiCoO_2$.

Interaction	A (eV)	ρ (Å)	C (eVÅ^6)
Li^+ - O^{2-}	426.48	0.3	0.0
Co^{3+} - O^{2-}	1329.82	0.3087	0.0
O^{2-} - O^{2-}	22764.3	0.1490	43.0

* Shell model: O^{2-} Y = -2.96, k = 57.0 eV/Å^2; Co^{2+} Y = 1.04, k = 196.30 eV/Å^2.

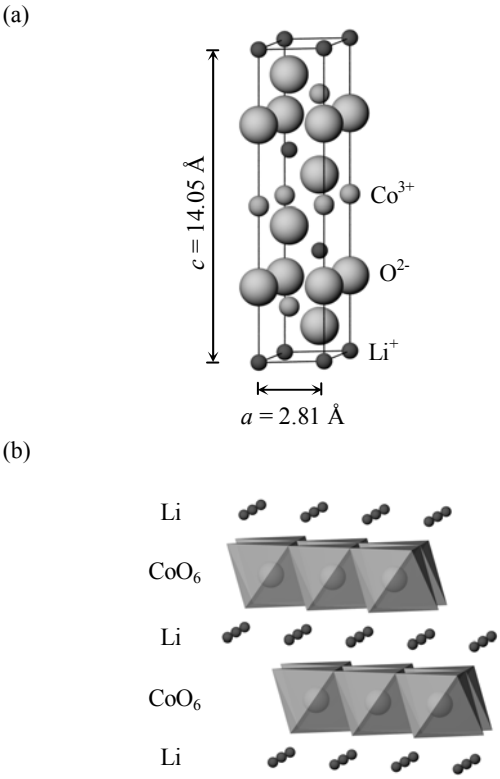

Fig. 1. Crystal structure of $LiCoO_2$; (a) hexagonal unit cell (S.G. $R\bar{3}m$); (b) layers of CoO_6 octahedra intercalated by Li ions.

The orthophosphates have an olivine-type structure with orthorhombic symmetry; the Li ions are aligned in 1D channels formed by corner- and edge-sharing MO$_6$ and PO$_4$ polyhedra (Fig. 2). Our potential model reproduced the experimental crystal structures of these compounds extremely well, as evidenced by the plot of lattice parameters versus transition metal cation (Fig. 3). The linear contraction across the period may be interpreted as an extension of Vegard's law, consistent with the mutual solubility between the four compounds.

Table II. Calculated and experimental structural parameters of $LiCoO_2$.

Parameter	Simulation	Experiment[19)]
a (Å)	2.81	2.82
c (Å)	14.05	13.92
Lattice energy (eV)	-95.84	-

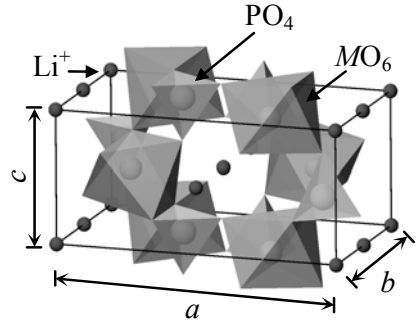

Fig. 2. Olivine-type crystal structure of Li*M*PO_4 (S.G.*Pnma*) showing *M*O_6 octahedral and PO_4 tetrahedral units.

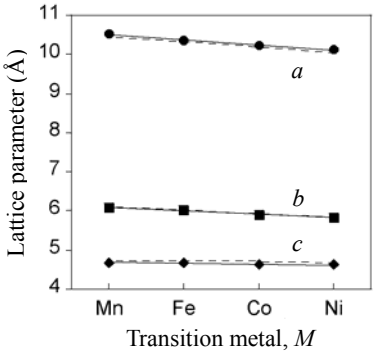

Fig. 3. Lattice parameters of Li*M*PO_4 (S.G. *Pmna*) as a function of transition metal *M* = Mn, Fe, Co and Ni, showing contraction across the period. Calculated values are indicated by points and connected by solid lines; experimental values[20-22)] are connected by dashed lines.

3.2 Intrinsic disorder

Defect energies were calculated for a number of different intrinsic disorder types based on equations maintaining overall charge neutrality. The results are summarized in Table III. These show that in $LiCoO_2$, the most energetically favorable defect type is Li deficiency, represented using Kröger-Vink notation as

$$2\mathrm{Li}_{\mathrm{Li}}^{\times} + \frac{1}{2}\mathrm{O}_2 \rightarrow 2V_{\mathrm{Li}}^{'} + 2h^{\bullet} + \mathrm{Li}_2\mathrm{O}. \qquad (4)$$

This indicates that the material will tend to contain Li vacancies compensated by hole species in the form of small polarons on Co sites (Co^{4+}). One consequence of this is that preparation of ideally stoichiometric $LiCoO_2$ can be expected to be difficult. On the other hand, electrochemical charging of an $LiCoO_2$-containing battery (i.e., de-intercalation of Li) should occur readily. The next most energetically favorable defect type is Li/Co site interchange; while the energy is not particularly low, it does suggest a small concentration of Li ions in the octahedral layers, and Co ions in the Li layer, which may degrade the cathode capacity slightly.

Table III. Energies of various defect types in $LiCoO_2$.

Disorder type	Energy (eV)
Li Frenkel	9.87
Co Frenkel	21.74
O Frenkel	9.01
Full Schottky	13.56
Li partial Schottky	7.72
Co partial Schottky	20.5
Li/Co antisite	2.79
Li^+ deficiency	0.68
Co^{2+} excess	10.66

In contrast to $LiCoO_2$, the olivine phosphates show much better resistance to non-stoichiometry, indicative of chemical stability resulting from the presence of the phosphate groups (Table IV). The most energetically favorable disorder type in this case is Li/*M* intersite exchange (i.e., cation antisite) defects,[16,23)] which can be represented in Kröger-Vink notation as

$$\mathrm{Li}_{\mathrm{Li}}^{\times} + M_M^{\times} \rightarrow \mathrm{Li}_M^{'} + M_{\mathrm{Li}}^{\bullet}. \qquad (5)$$

This can be rationalized by the similar coordination environments and free volumes of the two cation positions in the olivine structure, and has been confirmed experimentally using scanning transmission electron microscopy.[24)] Similar to $LiCoO_2$, this will affect the capacity of the material. It can be expected to have a more detrimental effect on the Li-ion conductivity in this case, since in the olivine phosphate materials Li migration is known to be one dimensional.[12,16,23)] This will be discussed further in the following section.

3.3 Li-ion diffusion

In the dilute limit, Li-ion diffusion in $LiCoO_2$ can be approximated as a vacancy hopping between adjacent lattice sites. Probing of the energy surface as a vacancy moves from one Li site to its neighbor produced the migration profile shown in Fig. 4, with a migration barrier at the saddle point of 0.48 eV. This relatively low value is consistent with the good Li-ion conductivity measured experimentally for $LiCoO_2$. The lowest energy pathway corresponds to a direct linear jump between Li lattice sites separated by 2.84 Å. It should be noted, however, that as Li ions are de-intercalated from the Li layer, the concentration of vacancies will

increase, with a corresponding increase in the likelihood of cooperative diffusion mechanisms and pathways becoming important. Nevertheless, our calculated value gives what is possibly the upper limit for the migration barrier, and is thus a reasonable indicator of the propensity for Li-ion conductivity.

Table IV. Energies of various defect types in LiMPO$_4$ (M = Mn, Fe, Co and Ni).

	Energy (eV)			
Disorder type	Mn	Fe	Co	Ni
Li Frenkel	1.97	2.15	2.32	2.38
M Frenkel	6.80	5.58	6.29	6.35
O Frenkel	7.32	5.46	6.71	8.65
Full Schottky	33.58	25.30	29.96	33.20
Li partial Schottky	7.36	6.33	6.97	6.95
M partial Schottky	7.15	5.58	6.21	6.77
Li/M antisite	1.48	1.13	1.18	1.17
Li^+ deficiency	8.97	4.41	5.27	7.58
M^{2+} excess	3.14	3.13	3.38	3.55

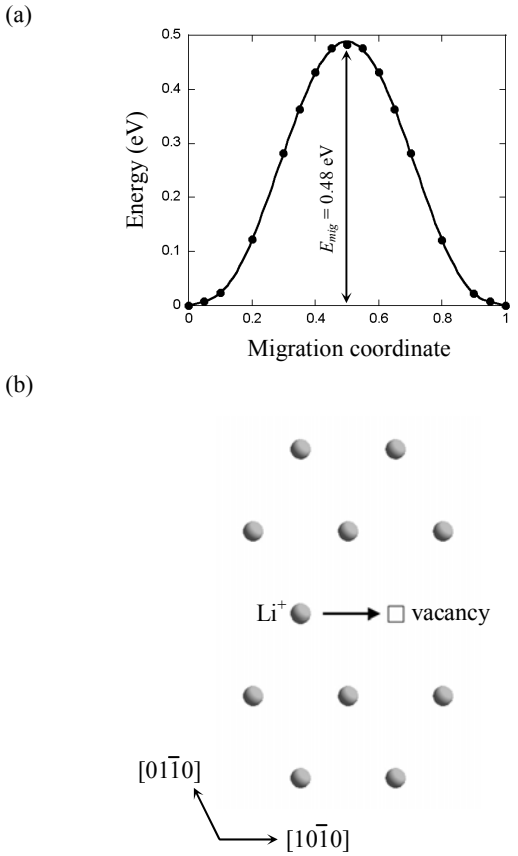

Fig. 4. (a) Energy profile for Li vacancy hopping mechanism in the $[10\bar{1}0]$ direction in $LiCoO_2$; (b) Li migration path in Li ion layer viewed down [0001].

The anisotropy of the olivine structure of the orthophosphates means that three different migration paths for the Li ion needed to be considered. Of these, migration down the [010] channel was found to have the lowest energy barrier (Fig. 5). This involved jumps of Li vacancies between lattice sites separated by 2.92 to 3.04 Å. In contrast to the layered $LiCoO_2$ material, however, migration was revealed to follow a curved trajectory (Fig. 5b).

It is interesting to note that the migration barrier decreases as the lattice parameters (and hence unit cell volume) decrease (Fig. 3), when normally the opposite is expected (particularly for larger diffusing species, such as oxide ions). The current result suggests, rather, that there is an optimum lattice volume or bottleneck size for ion diffusion. It should be noted, however, that other factors, such as bond strengths and defect binding energies, will also strongly influence the overall ion conductivities.

The large difference in energy barriers between the three pathways considered[16] in the olivine phosphates indicates that ionic conductivity in this family of compounds is essentially one dimensional, as has since been confirmed experimentally.[25] This one-dimensionality has two immediate implications. In order to maximize cathode performance it is desirable to i) reduce the amount of antisite disorder (M ions on Li sites), and ii) increase the proportion of (010) surface in the particle morphology of LiMPO$_4$ powders.

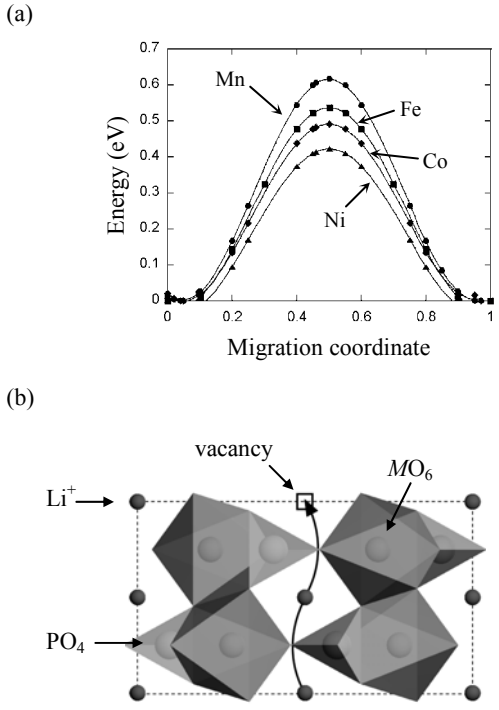

Fig. 5. (a) Energy profiles for Li vacancy hopping mechanism along [010] in LiMPO$_4$ (M = Mn, Fe, Co, Ni); (b) curved Li migration path viewed down [001].

3.4 Surfaces and crystal morphologies

Several low index surfaces of $LiCoO_2$ were simulated and their energies calculated according to eq. 3. Analysis of the surface energies, reported in Table V, shows that the most stable surface is the basal plane, (0001), followed by the

$(10\bar{1}4)$ surface, in fair agreement with recent *ab initio* calculations of the same system.[26] Consequently the $\{10\bar{1}4\}$ and $\{0001\}$ family of planes dominate the calculated equilibrium morphology (Fig. 6a). However, the (0001) surface is impermeable to Li-ion diffusion, so that intercalation/de-intercalation of Li ions within the 2D Li layers parallel to (0001) must take place through the other surfaces. Altering the surface chemistry of $LiCoO_2$ particles to minimize expression of the (0001) surface and increase the number of surfaces normal to (or strongly inclined to) the conduction plane should help optimize battery charge-discharge rates.

Table V. Surface energies of various low index planes of $LiCoO_2$.

Plane	Surface Energy (Jm^{-2})
(0001)	1.38
(10-10)	3.13
(01-11)	2.56
(10-11)	2.26
(11-20)	2.95
(11-21)	2.77
(01-12)	3.75
(02-21)	3.01
(10-12)	2.42
(11-21)	2.67
(10-14)	1.45
(14-50)	2.86

For $LiFePO_4$, all planes with indices $h,k,l \leq 2$ were examined, giving a total of 19 different surfaces, representing a larger survey than had been carried out previously.[14] Phosphate groups were kept intact to maintain charge neutrality. The olivine structure necessitates that stable slices can only be formed when all three moieties (Li^+, Fe^{2+} and PO_4^{3+}) were present in stoichiometric ratios in the surface layer. The much greater size of the phosphate unit compared to the other two ions also means that all surfaces are relatively uneven on the atomic scale.

Table VI. Surface energies of various low index planes of $LiFePO_4$.

Plane	Surface Energy (Jm^{-2})	Plane	Surface Energy (Jm^{-2})
(001)	1.11	(120)	0.86
(010)	0.72	(201)	0.71
(100)	0.87	(210)	0.90
(011)	0.75	(112)	0.88
(101)	0.88	(121)	0.94
(110)	0.92	(211)	0.80
(111)	0.89	(122)	0.80
(012)	1.02	(212)	0.86
(021)	0.82	(221)	0.79
(102)	1.15		

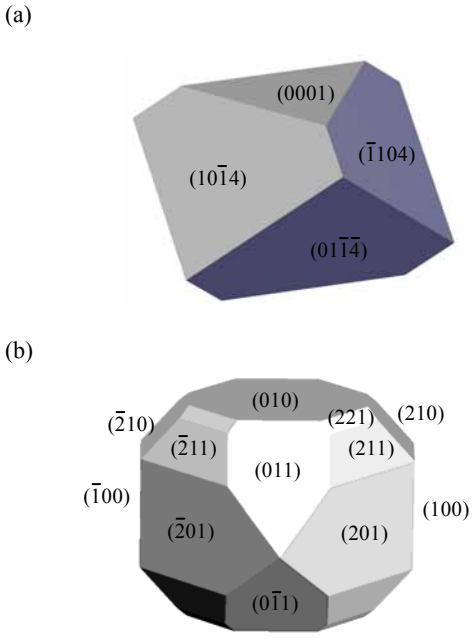

Fig. 6. Equilibrium crystal morphologies for (a) $LiCoO_2$, and (b) $LiFePO_4$.

For many crystal orientations, different dipole-free surfaces are possible by cutting the crystal at different positions; Table VI lists the energies for the most stable terminating layers, that is, those slices with the lowest surface energy after relaxation. As expected, relaxation was most severe in the uppermost one or two layers, with tilting of phosphate tetrahedra and re-positioning of cations in many cases. Low energy slices were found for (010), (011) and (201) surfaces. Similar trends in surface energies and crystal shape can be expected for the Mn, Co and Ni analogs, given their similar structures and interatomic bonding. The (010) surface is of particular interest in these materials because it lies normal to the direction of Li-ion diffusion. Careful control of the surface chemistry and other kinetic factors by varying synthesis conditions, for example, can prove useful in maximizing the (010) surface area.[27]

4. Conclusions

The defect energetics, ion migration mechanisms, surface energies and crystal morphologies of lithium ion battery cathode materials $LiCoO_2$ and $LiMPO_4$ (M = Mn, Fe, Co or Ni) have been examined using atomistic simulation techniques based on the Born model of ionic solids. The simulations reveal the following:

1) The lowest energy disorder types comprise cation antisite defects in the $LiMPO_4$ orthophosphates and lithium deficiency in $LiCoO_2$. The latter reflects the lower stability of the layered structure compared with the orthophosphates.
2) Lithium diffusion in $LiCoO_2$ is two dimensional, and restricted to within Li layers with an activation barrier of 0.45 eV. In $LiMPO_4$ materials diffusion is one dimensional only, with barriers ranging from 0.44 eV to 0.62 eV down [010] channels.

3) Unlike the direct linear path observed in $LiCoO_2$, in the orthophosphates the Li ion follows a curved path between lattice vacancies.
4) Low index, low energy surfaces of stoichiometric $LiCoO_2$ and $LiFePO_4$ require lithium deficiency to be stable. In both cases, modification of surface chemistry is desirable to maximize intercalation/de-intercalation rates.

Acknowledgments

Part of this study was funded by the Engineering and Physical Sciences Research Council (EPSRC), U.K. The authors thank C. Masquelier, T. J. Richardson and A. Kuwabara for helpful discussions.

1) J. M. Tarascon and M. Armand: Nature **414** (2001) 359.
2) K. Mizushima, P. C. Jones, P. J. Wiseman and J. B. Goodenough: Mater. Res. Bull. **15** (1980) 783.
3) J. B. Goodenough: J. Power Sources **174** (2007) 996.
4) A. K. Padhi, K. S. Nanjundaswamy and J. B. Goodenough: J. Electrochem. Soc. **144** (1997) 1188.
5) B. Kang and G. Ceder: Nature **458** (2009) 190.
6) B. Ammundsen, J. Roziére and M. S. Islam: J. Phys. Chem. B **101** (1997) 8156.
7) N. Kuganathan and M. S. Islam: Chem. Mater. **21** (2009) 5196.
8) D. Carlier, A. Van der Ven, C. Delmas and G. Ceder: Chem. Mater. **15** (2003) 2651.
9) J. M. Osorio-Guillén, B. Holm, R. Ahuja and B. Johansson: Solid State Ion. **167** (2004) 221.
10) C. Y. Ouyang, S. Q. Shi, Z. X. Wang, H. Li, X. J. Huang and L. Q. Chen: J. Phys.: Condens. Matter **16** (2004) 2265.
11) O. Le Bacq and A. Pasturel: Phil. Mag. **85** (2005) 1747.
12) D. Morgan, A. Van der Ven and G. Ceder: Electrochem. Solid State Lett. **7** (2004) A30.
13) T. Maxisch, F. Zhou and G. Ceder: Phys. Rev. B **73** (2006) 104301.
14) L. Wang, F. Zhou, Y. S. Meng and G. Ceder: Phys. Rev. B **76** (2007) 165435.
15) B. G. Dick and A. W. Overhauser: Phys. Rev. **112** (1958) 90.
16) C. A. J. Fisher, V. M. Hart Prieto and M. S. Islam: Chem. Mater. **20** (2008) 5907.
17) C. A. J. Fisher and M. S. Islam: J. Mater. Chem. **18** (2008) 1209.
18) J. D. Gale and A. L. Rohl: Mol. Simul. **29** (2003) 291.
19) M. Holzapfel, C. Haak and A. Ott: J. Solid State Chem. **156** (2001) 470.
20) O. García-Moreno, M. Alvarez-Vega, F. García-Alvarado, J. García-Jaca, J. M. Gallardo-Amores, M. L. Sanjuán and U. Amador: Chem. Mater. **13** (2001) 1570.
21) G. Rousse, J. Rodriguez-Carvajal, S. Patoux and C. Masquelier: Chem. Mater. **15** (2003) 4082.
22) F. Kubel: Z. Kristallogr. **209** (1994) 755.
23) M. S. Islam, D. J. Driscoll, C. A. J. Fisher and P. R. Slater: Chem. Mater. **17** (2005) 5085.
24) S.-Y. Chung, S.-Y. Choi, T. Yamamoto and Y. Ikuhara.: Phys. Rev. Lett. **100** (2008) 125502.
25) S. Nishimura, G. Kobayashi, K. Ohoyama, R. Kanno, M. Yashima and A. Yamada: Nature Mater. **7** (2008) 707.
26) D. Kramer and G. Ceder: Chem. Mater. **21** (2009) 3799.
27) G. Chen, X. Song and T. J. Richardson: Electrochem. Solid State Lett. **9** (2006) A295.